INSTITUTE OF PHYSICS PUBLISHING JOURNAL OF PHYSICS: CONDENSED MATTER

J. Phys.: Condens. Matter **13** (2001) 5937–5946 www.iop.org/Journals/cm PII: S0953-8984(01)23264-0

Positron annihilation and transmission electron microscopy study of the evolution of microstructure in cold-rolled and nitrided FeNiTi foils

N G Chechenin[1], A van Veen[2], R Escobar Galindo[2], H Schut[2], A R Chezan[1], P M Bronsveld[3], J Th M de Hosson[3] and D O Boerma[1]

[1] Nuclear Solid State Physics Laboratory, Materials Science Centre, University of Groningen, Nijenborg 4, NL-9747 AG Groningen, The Netherlands
[2] Interfaculty Reactor Institute, Delft University of Technology, Mekelweg 15, NL-2629 JB Delft, The Netherlands
[3] Department of Applied Physics, Materials Science Centre, University of Groningen, Nijenborg 4, NL-9747 AG Groningen, The Netherlands

Received 22 March 2001, in final form 15 May 2001

Abstract

Positron beam analysis (PBA) and transmission electron microscopy (TEM) were applied to study structural transformations in cold-rolled $Fe_{0.94}Ni_{0.04}Ti_{0.02}$ foils, which were subjected to different thermal treatments in an atmosphere of a gas mixture of $NH_3 + H_2$ (nitriding). Positrons proved to be sensitive probes for the microstructure evolution and formation of nitride precipitates. The nitriding of the samples in the α-region (αN) of the Lehrer diagram for the Fe–N system produced a large decrease of the central part of the Doppler broadened annihilation γ-peak (S-parameter) and an increase of the contribution to the wings of the peak (W-parameter). The effect, ascribed to replacing of vacancy type positron traps by nitride-related traps, was much more pronounced for the α-nitrided samples than for samples annealed in vacuum at the same temperature. A reduction of the αN samples by annealing in H_2 atmosphere brings the S-parameter back to a higher value. Further nitriding of αN samples in the γ'-region (αN + γ'N) of the Lehrer diagram increases S and lowers the W-parameter compared with the αN samples. The changes in S- and W-parameters are interpreted on the basis of the evolution of microstructure of the films during the processing.

1. Introduction

During gaseous nitriding of iron alloys, precipitates of nitrides of the alloying elements are often formed [1–7], influencing the important physical properties of the alloy. In addition to the precipitates of nitrides of alloying elements, also the desirable Fe–N phases can be produced in the material. As can be seen from the Lehrer diagram, shown in figure 1, the Fe–N phases can be obtained in thermal equilibrium conditions at a fixed temperature by applying different

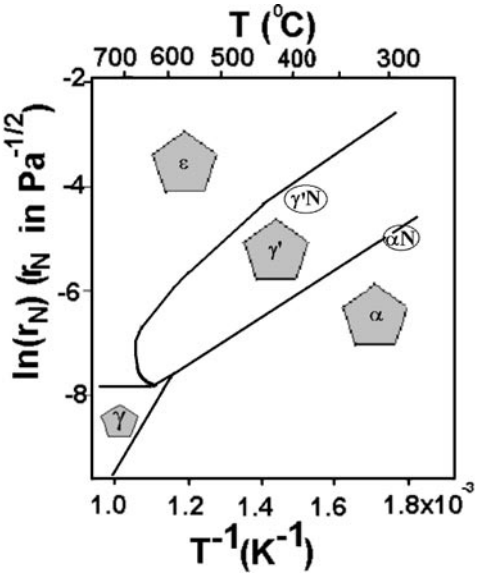

Figure 1. Lehrer diagram for the binary Fe–N system.

nitriding potentials [8–10], $\ln(r_N) = \ln[p(\mathrm{NH_3})/p(\mathrm{H_2})^{3/2}]$, where $p(\mathrm{NH_3})$ and $p(\mathrm{H_2})$ are the pressures of ammonia and hydrogen, respectively.

The purpose of present work was to investigate the evolution of the microstructure in the foils with an extremely high initial concentration of defects during a rather soft thermal treatment, i.e. moderate temperatures, combined with nitriding. Here we report on the evolution of the microstructure in cold-rolled films, subjected to a nitriding in the α- and in the γ'-regions and to a subsequent reduction in a hydrogen atmosphere. The results presented were mainly obtained using two techniques, PBA and TEM. The experimentally measured parameters of PBA are sensitive to positron trapping defects, like vacancies, to the momentum distribution and concentration of electrons averaged over the surface area of 1 mm in diameter. In contrast, TEM characterizes the microstructure on the μm and nm scale. The mutually complementary techniques allow a deeper insight into the evolution of defects in the nitrided material.

2. Experiment

2.1. Sample preparation

Slices (0.5 mm thick) of the bulk Fe + Ni(4 at.%) + Ti(2 at.%) alloy (99.9% pure, MaTeck GmbH) were cold rolled (rl) in two perpendicular directions to 2–4 μm thick foils, i.e. by introducing more than 99% deformation. Subsequently, the foils were nitrided during a period between 1 and 24 hours at a temperature in the range 350–400 °C in a $\mathrm{NH_3} + \mathrm{H_2}$ mixture of 1 atm. We call this process α-nitriding (αN), if the nitriding potential $\ln(r_N)$, and the temperature T correspond to the α-region of the Fe–N Lehrer phase diagram [6, 7], figure 1, so that no formation of stoichiometric Fe nitrides is expected. Alternatively, the nitriding process is called γ'N-nitriding, when $\ln(r_N)$ and T are in the γ'-regions, respectively. In general, we obtained phases according to the Lehrer diagram, and, up to now, the effect of alloying elements, Ti and Ni, on the nitriding process has not been clearly established in the applied range of composition. The regimes, applied in this work, are marked in figure 1 as αN and γ'N. Some of the samples after nitriding were reduced (rd) in a hydrogen atmosphere at $T = 300$–

600 °C. As measured by the elastic recoil detection (ERD) technique, the concentration of carbon and oxygen in the foils and nitrogen in the as-rolled foils at a depth higher than 10 nm was below 0.1 at.%.

2.2. Analysis techniques

A positron beam based on a 40 mCi ^{22}Na source was used. After moderation by a 6 μm tungsten foil a positron current of 5×10^4 positrons s^{-1} was obtained and the energy was varied between 1 and 30 keV in the PBA analysis. Annihilation γ-quanta, measured by a Ge detector, produce a peak centred on an energy of $E_\gamma = 511$ keV. The broadening of the peak is determined by the Doppler effect, i.e. $\Delta E = pc/2$. Here c is the light velocity and p is the momentum of the electrons, which depends on the site of annihilation. The shape of the peak is characterized by the S- and W-parameters [10]. The main contribution to the central area of the peak (S) is due to low-momentum valence and unbound electrons, while the wings (W) are due to high-momentum core electrons. Thus the S-value will be higher for a material with a lower average atomic number Z or with a higher concentration of vacancy type defects. For the W-parameter this relation is reversed. In general, positrons trap at sites with low atomic density in a material, e.g. vacancies, vacancy clusters, open-volume sites at interfaces and kinks at dislocations. The annihilation characteristics depend also on the presence of gases and the nature of the atoms surrounding the trapping site [10].

For the TEM study, CTEM JEM 200CX and HRTEM JEM 4000 EX/II electron microscopes were used with electron beam energies of 200 and 400 keV, respectively. Before inspection in TEM, the samples were thinned by two-beam ion milling until perforation. Normally, after milling the samples were exposed to air for a period less than 5–10 minutes. Still, in some cases, oxidation of the surface was observed in TEM diffraction patterns.

The texture and phase composition of the samples were characterized by XRD, using a Philips PW1710 spectrometer for 1D ϑ–2ϑ scans and a Philips X'Pert MRD system for 2D scans.

3. Results and discussion

In figure 2 the S- and W-values versus the positron energy E are plotted for FeNiTi samples with different treatments. At low positron implantation energies S-values are high and W-parameters are low, due to back-diffusion of the positrons to the surface and annihilation with a higher density of loosely bound electrons in the near-surface region [10]. Positrons with higher energies penetrate to a larger depth where the density of defects is almost constant and $S(E)$ and $W(E)$ show a plateau. The $S(E)$ and $W(E)$ data were fitted separately, using the VEPFIT program [11]. In the program the positron diffusion is described using two sets of parameters, one set for the near-surface region and another one for the bulk. Two variables in each set were a diffusion length and S or W. Since it is difficult to take into account the surface oxidation, which is always present, we will discuss only the behaviour of S- and W- parameters for the bulk of the material, corresponding to $E > 5$ keV, where the fit yielded a constant value.

In table 1 the results of the fits are listed. In the second column the abbreviations rl, rd, αN, γ'N are used to note treatments, cold rolling, reduction (in H_2 atmosphere) and nitriding in α- and in γ'-regions of the Lehrer diagram, respectively. Also the temperature and exposition time in hours are given. In the table also the S–W parameters are given, which are characteristic for the annihilation in the different samples. Since the S and W values are averaged over a large number of points, the experimental errors are below ± 0.0005 and $\pm 0.000\,05$ for S and W, respectively, i.e. the last digits in the values of both S and W, listed in the table, are reliable.

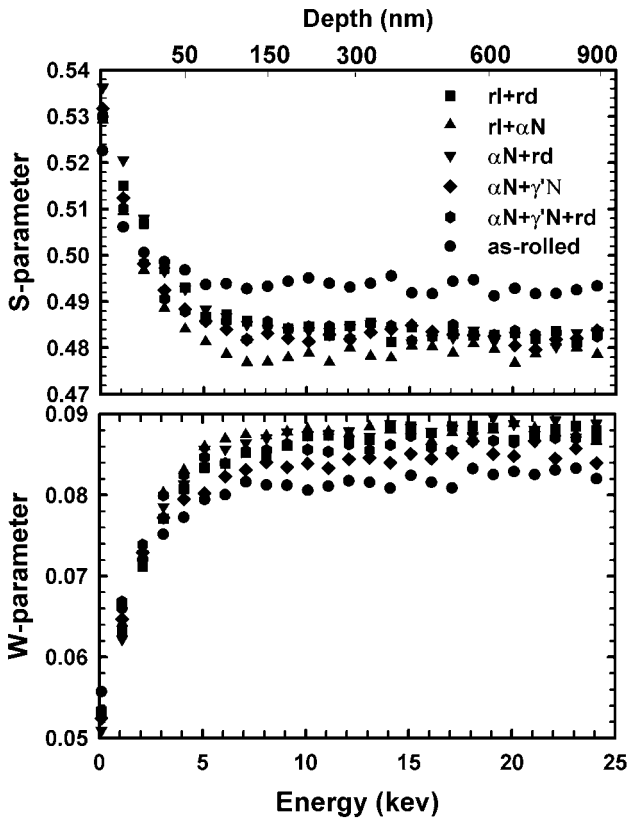

Figure 2. The dependence of *S*- and *W*-parameters on the energy of positrons for different treatment of the FeNiTi foils.

Table 1. Positron annihilation *S*- and *W*-parameters for the as-rolled and nitrided samples.

No	Sample No and treatment	*S*	*W*	Positron trapping sites
1.	97: as-rolled (rl)	0.493	0.0820	Vacancies, vacancy clusters, dislocations, substitutional Ti
2.	98: rl + rd, 300 °C, 20 h	0.483	0.0879	Vacancies removed, rearranged dislocations, substitutional Ti
3.	95a: rl + αN, 300 °C, 20 h	0.479	0.0879	No vacancies, rearranged dislocations, TiN/αFe(N) interfaces cured by excess N
4.	93c: as 95a + rd, 300 °C, 20 h, H_2	0.482	0.0883	No vacancies, reduced dislocations, TiN/Fe interfaces, no excess N
5.	96: as 95a+ γ'N, 380 °C,	0.482	0.0850	No vacancies, residual dislocations, TiN/αFe(N), 4 h TiN/γ' and γ'N/αFe(N) interfaces in 35% γ'N-phase
6.	94: as 96 + rd, 380 °C,4 h	0.483	0.0864	As 5, but interface trapping sites exempt of nitrogen

Evolution of possible trapping sites, which is briefly summarized in the last column, will be discussed in the following.

In figure 3 the *S*–*W* parameters are plotted in a so-called *S*–*W* map [10] and the routes

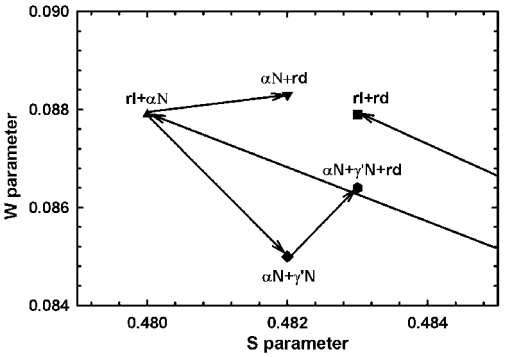

Figure 3. *S*–*W* cluster point plot. The points correspond to the mean *S*- and *W*-values in the bulk, where they saturate for the positron energy above 5 keV. The level of saturation depends on the momentum distribution of the electrons at a given depth.

from point to point are indicated, which correspond to the different treatments. From the data in figures 2 and 3 and table 1 one can see that the as-rolled foils have the highest *S*- and the lowest *W*-values. This is expected because during the severe plastic deformation many vacancies and dislocations are generated, which trap positrons. A TEM dark field (DF) image for the as-rolled sample is shown in figure 4(a). One can see the white-dot contrast, where a dark background is due to a high defect density induced by cold rolling. Slip bands are also seen as wide (200–400 nm) bands across the image.

A common procedure to remove defects is a thermal treatment. Indeed, when the sample after rolling was annealed in a hydrogen atmosphere at 300 °C for 20 hours, *S* decreased and *W* increased, indicating a decrease of the concentration of low-momentum electrons mainly due to annihilation of point defects and a partial recovery of the highly distorted crystal structure. However, the lowest value of *S* and one of the highest *W*-values was obtained when the sample was α-nitrided. One can see from the data, e.g. figure 3, that the *S*-value in the (rl+αN) sample is significantly less than for the reduced (rl + rd) sample, though the treatment temperature and time were the same. As evidence for the change in the microstructure during α-nitriding at as low temperature as 300 °C, in figure 4(b) one can observe that the defects, producing the contrast in the DF image, predominantly rearrange in lines, running perpendicular to the $\boldsymbol{g}_{\{200\}\alpha\mathrm{Fe}}$-vector chosen for the DF. Apparently, this substructure was created during an initial stage of the recovery process, which is stimulated at this low temperature by nitriding [12]. Such a nitrogen-assisted recovery of defects results in trapping sites for the positrons which are saturated with nitrogen so that a higher probability for annihilation with high-momentum core electrons exists than for empty sites.

An important contribution to the general picture of evolution of the microstructure comes from the process of formation of TiN precipitates. In diffraction patterns, shown in figure 5(a), one can observe weak and diffuse streaks, running from {200} to the centre spot. This is in accordance with earlier observations that these fcc precipitates form on the matrix bcc cube faces with the Bain orientation relationship (Bain OR): (100)bcc $\parallel$ (100)fcc and [001]bcc $\parallel$ [01$\bar{1}$]fcc [1–7]. The misfit in the interface plane (100), $\varepsilon_{\parallel} = (a_{TiN}/\sqrt{2} - a_{\alpha Fe})/a_{\alpha Fe} = 0.046$ is small, but in the perpendicular direction the misfits, $\varepsilon_{\perp} = (a_{TiN} - a_{\alpha Fe})/a_{\alpha Fe} = 0.48$ are large, favouring the thin platelet shape of the precipitates. The presence of the streaks indicates that the thickness of the precipitates is of the order of the lattice parameter, i.e. $\approx$0.2 nm. The weakness/diffuse character of the streaks shows that the precipitates are not only thin, but also narrow, i.e. precipitates are small in at least two directions. The weight measurements of the samples before and after nitriding reveal a large concentration of absorbed nitrogen, about 3.5 times more than required for the stoichiometric TiN composition [13]. From XRD we observe that the lattice is uniformly dilated, resulting in an increase of the lattice parameter

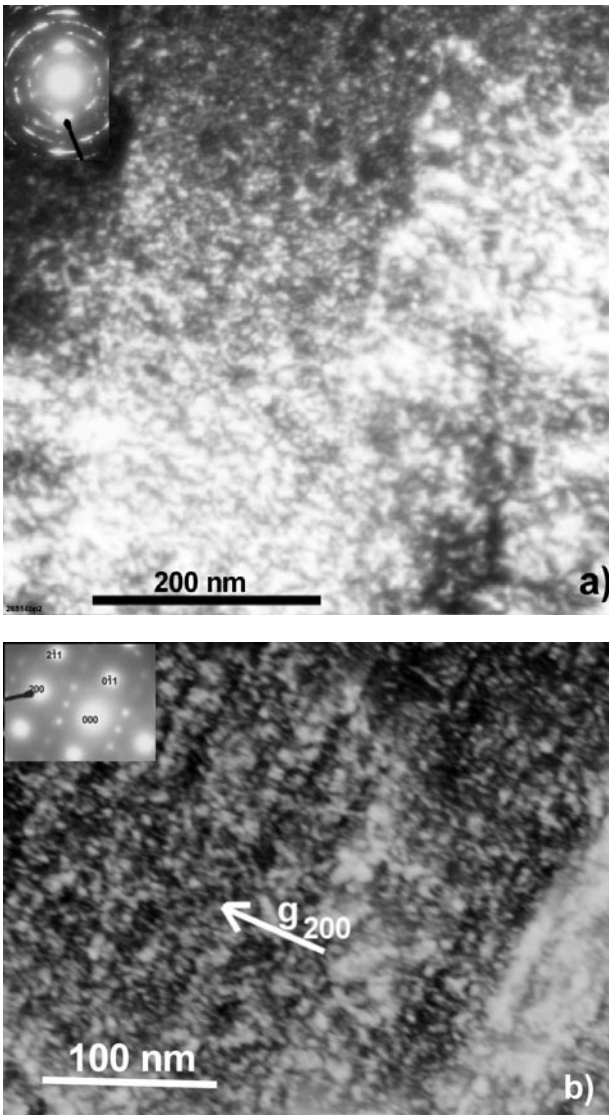

Figure 4. TEM DF images of as-rolled (a) and α-nitrided (b) samples. The corresponding diffraction patterns are shown in the insets.

from $a = 0.287$ nm (αFe) to $a = 0.293$ nm. This uniform strain is believed to be caused by an adaptation of the αFe lattice to the lattice parameter of the precipitates, since the distance between the platelike precipitates is small, of the order of 3 nm, for the platelets with the volume of the order of 1 nm^3, i.e. of one monolayer thick and several cell units wide. The relation between the lattice parameter and the excess nitrogen content is in accordance with the Vigard-type relation [6, 13], implying that the lattice dilation may be promoted by the dissolved nitrogen. This picture is in good accordance with the results of PBA in figure 3, where the decrease of S for the rl + αN point, compared with the rl + rd point, means that the formation of the precipitates during α-nitriding does not introduce additional (necessary) dislocations, i.e. these precipitates are coherent. It also means that the platelets are thin, otherwise, due to

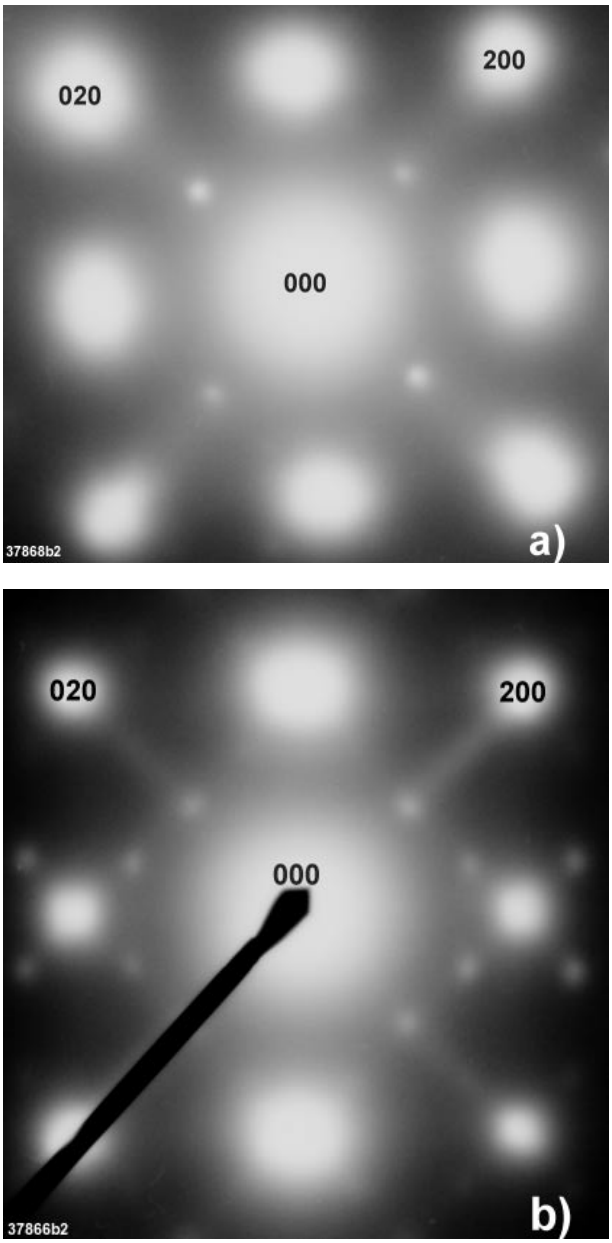

Figure 5. Diffraction patterns of α-nitrided (a) and reduced (b) samples, showing the evolution of {020} streaking, which becomes more pronounced after the reduction.

the large perpendicular misfit, there could be no coherency.

The effect of α-nitriding on the W-parameter is not stronger than that of annealing of cold-rolled foils in hydrogen atmosphere, in contrast to the S-parameter. That is because the W-parameter is sensitive to the average Z of the surrounding atoms. An increase of the N concentration in trapping sites leads to an increased overlap of the positron wavefunction with core electrons of N and thus an increase of W. This increase is, of course, less than expected

for overlap with heavier atoms.

A reduction of the αN samples removes the excess nitrogen from the bcc matrix, keeping the nitrogen content in the TiN precipitates unchanged. As follows from figures 2 and 3 and table 1, the reduction brings the S back to a higher value, proving that the presence of the excess nitrogen plays an essential role. On the one hand the removal of nitrogen from positron trapping sites lowers the mean electron velocity in these sites. On the other hand the removal of nitrogen could lead to a loss of coherency between the precipitates and the matrix, resulting in more defects, like stacking faults. It is shown in figure 5(b) that the reduction makes the streaks in the diffraction pattern narrower and sharper, indicating that the precipitates grew larger (wider, but not thicker). Furthermore, the TiN/αFe interface gained more contrast by removing the excess nitrogen. At the same time, the W-value is slightly increased, which is caused by an increase of the average Z of atoms in the material.

If, instead of the reduction, we continue to nitride the αN sample in the γ'-region then we also (as in the (αN+rd) samples) obtain a high S-value, while W decreases. According to XRD and Mössbauer spectroscopy results, the sample contains in that case about 35% of γ'-Fe_4N phase, which develops in a lamellar-type microstructure, as evidenced by TEM [14]. Compared with the (rl+αN) case, it is obvious that the lower W-parameter in (αN+γ'N) nitriding, figures 2 and 3, is connected with a higher N content. The increase of S indicates that the formation of the γ'-Fe_4N/αFe(N) interfaces leads to a larger disturbance in the coherency of the material than the formation of the TiN/αFe(N) interfaces, in spite of the fact that the γ'-Fe_4N phase has the fcc structure with similar lattice parameter as TiN. That the coherency in the matrix is disturbed by γ'-nitriding is illustrated in figure 6(a) by a high-resolution TEM (HRTEM) image in an area with dominating [111] orientation of αFe. The regular {110} bcc fringes are disturbed in many places: due to the presence of γ'-phase locally only one of three possible (110) fringes appears distinctly while the other two are smeared out as interpreted in figure 6(b), where a {111} αFe plane is schematically shown with an overlay of the γ'-Fe_4N precipitate, which follows the Bain OR. Several reasons for the poorer coherency could be referred to. The misfit at the {100} γ'/αFe interface, $\varepsilon_{\parallel} = (a_{\mathrm{fcc}} - a_{\mathrm{bcc}}\sqrt{2})/a_{\mathrm{bcc}}\sqrt{2} = (0.38 - 0.287\sqrt{2})/0.287\sqrt{2} = -0.064$, is somewhat larger than $\varepsilon_{\parallel} = 0.046$ for TiN/αFe interface. An evident reason is the much higher volume fraction and larger size of inclusions of γ'-phase, compared with TiN. Finally, the sample having 35% of second phase was in a stage of phase transition, thus one could expect a distortion of the microstructure, corresponding to a frustrated state, including additional transformation dislocations.

A reduction of the (αN + γ'N) samples, see the (αN + γ'N + rd) point in figure 3, increases both the S- and W-values. By the reduction we transform the γ'-phase back to the α-phase and remove excess nitrogen from the α-matrix. So, if the transformation were ideal, then the (αN + γ'N + rd) sample should have S and W at least close to those for the (αN + rd) sample. Possibly, even a smaller S might have occurred, because some more residual defects could annihilate during the additional thermal treatment during γ'-nitriding. From figure 3 we see that this is not the case, i.e. the back-transformation is not ideal. From our XRD data we can conclude that a tiny quantity of γ' is left, thus the removal of the nitrogen was not complete and that explains a smaller W-value. Since the S-value was also larger in this sample, compared to that of (αN+rd), apparently, during the cycle $\alpha \rightarrow \gamma' \rightarrow \alpha$ not all of the necessary dislocations were removed, but they had been built up at each sequential step.

4. Conclusions

In general, it has been found that positrons used to probe the iron films subject to nitriding processes trap effectively at the formed phases and precipitates. They are sensitive to misfit

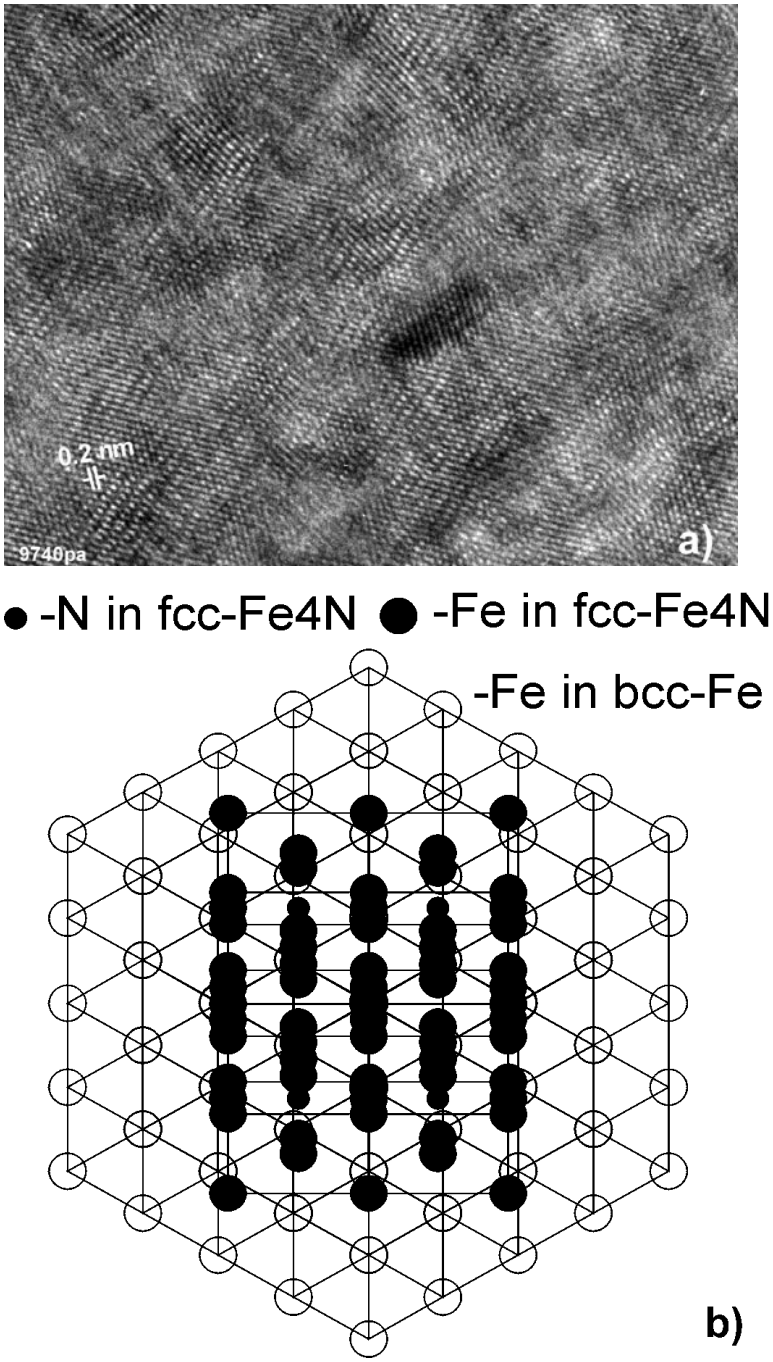

Figure 6. (a) HRTEM image of the sample, which was nitrided first in α-, then in γ'-regions, and which contains about 35% of γ'-Fe_4N phase. The patterns show a distorted nanostructure of α-Fe with a [111] pole: due to the presence of the γ'-phase locally only one of three possible (110) fringes appears distinctly while the other two are smeared out as interpreted in (b), where a {111} αFe plane is schematically shown (open circles) with an overlay of the γ'-Fe_4N precipitate, which follows the Bain OR.

defects and the presence of nitrogen interfacial areas. In the following the observations and interpretations are summarized.

(1) A reduction of as-rolled samples in H_2 atmosphere at a temperature of $T = 300\,^{\circ}$C leads to an annihilation of point defects and therefore to a decrease of S and an increase of W.
(2) Nitriding in the α-region of the Lehrer diagram for the Fe–N system leads to the largest recovery of the rolled material, observed as the smallest S-value and one of the highest W-values among the films investigated. The effect is ascribed to (a) thermal annealing of point defects, (b) formation of TiN precipitates, (c) a nitrogen-assisted recovery of defects and (d) a nitrogen-assisted release of strain on the TiN/Fe(N) interface.
(3) A reduction of αN samples removes the excess nitrogen and brings the sample to a higher S-value. This indicates a loss of coherency of TiN precipitates and formation of defects on the TiN/αFe interface. At the same time, the W-value is slightly increased, which is caused by an increase of the average Z of the material.
(4) Nitriding in the γ'-region brings S to a higher value while W decreases. An increase of S could be connected with the formation of γ'/αFe(N) interfaces which contain additional transformation dislocations. A decrease of W is explained by a decrease of the average electron density due to the formation of the Fe_4N phase.
(5) A reduction of the (αN + γ'N) samples does increase both S- and W-values. This observation shows that the back-transformation was not ideal. Besides the fact that a small quantity of γ' was left at the final step in the cycle $\alpha \rightarrow \gamma' \rightarrow \alpha$, also not all the transformation dislocations were removed in the following step in the sequence. Instead the dislocation density was increased.

Acknowledgments

This work is financially supported by the Dutch Technology Science Foundation (STW) project GWN.4561.

References

[1] Chechenin N G, Bronsveld P M, Chezan A, Craus C B, Boerma D O, de Hosson J Th M and Niesen L 2000 *Phys. Status Solidi* a **177** 117
[2] Phillips V A and Seybolt A U 1968 *Trans. Metall. Soc. AIME* **24** 2416
[3] Mortimer B, Grieveson P and Jack K H 1972 *Scand. J. Met.* **1** 203
[4] Jack D H 1976 *Acta Metall.* **24** 137
[5] Ronay M 1981 *Metall. Trans.* A **12** 1951
[6] Rickerby D S, Henderson S, Henry A and Jack K H 1986 *Acta Metall.* **34** 1687
[7] Somers M A, Lankreijer R M and Mittemeijer E J 1989 *Phil. Mag.* A **59** 353
[8] Kooi B J, Somers M A J and Mittemeijer E J 1996 *Metall. Mater. Trans.* **27** 1063
[9] du Marchie van Voorthuysen E H, Feddes B, Chechenin N G, Inia D K, Vredenberg A M and Boerma D O 2000 *Phys. Status Solidi* a **177** 127
[10] van Veen A, Schut H and Mijnarends P E 2000 *Positron Beams and their Applications* ed P G Coleman (Singapore: World Scientific) p 191–225
[11] van Veen A, Schut H, de Vries J, Hakvoort R A and Ijpma M R 1990 *AIP Conf. Proc.* **218** 171
[12] Li J C M 1966 Recovery process in metals *Recrystallization, Grain Growth and Textures* ed H Margolin (Metals Park, OH: AMS)
[13] Chezan A R, Chechenin N G, Bronsveld P M, Craus C B, Boerma D O, de Hosson J Th M and Niesen L 2001 *Metall. Mater. Trans.* A submitted
[14] Chechenin N G, Bronsveld P M, Chezan A R, Craus C B, Boerma D O, de Hosson J Th M and Niesen L 2000 *MRS Proc. Fall 2000 Symp. on Influences of Interface and Dislocation Behaviour on Microstructure Evolution* vol 652 at press